Giant electrostrain via field induced structural transformation in Sm doped BiFeO3-PbTiO3 ceramics revealed by in-situ synchronous X-ray diffraction

WANG, Xinzhen, ZUBAIRI, Hareem, SJÖKVIST, Robin <http://orcid.org/0000-0001-5571-2986>, WASIM, Muhammad, LIU, Xiaojiao, KLEPPE, Annette K <http://orcid.org/0000-0002-0258-3241>, FETEIRA, Antonio <http://orcid.org/0000-0001-8151-7009>, BEANLAND, Richard, WANG, Ge <http://orcid.org/0000-0003-1842-8067> and REANEY, Ian M

Acta Materialia 316 (2026) 122480

Contents lists available at ScienceDirect

Acta Materialia

journal homepage: www.elsevier.com/locate/actamat

Full length article

Giant electrostrain via field induced structural transformation in Sm doped $BiFeO_3$-$PbTiO_3$ ceramics revealed by in-situ synchronous X-ray diffraction

Xinzhen Wang [a,b], Hareem Zubairi [c], Robin Sjökvist [d], Muhammad Wasim [e], Xiaojiao Liu [f], Annette K. Kleppe [f], Antonio Feteira [e], Richard Beanland [d], Ge Wang [c,*], Ian M Reaney [b,*]

[a] College of Materials Science and Engineering, Shandong University of Science and Technology, Qingdao, Shandong, 266590, China
[b] School of Chemical, Materials and Biological Engineering, University of Sheffield, Sheffield, UK
[c] Department of Materials, University of Manchester, Manchester, UK
[d] Department of Physics, University of Warwick, Coventry, UK
[e] School of Engineering and Built Environment, Sheffield Hallam University, Sheffield, S1 1WB, UK
[f] Diamond Light Source, Harwell Science and Innovation Campus, Didcot, OX11 0DE, UK

ARTICLE INFO

Keywords:
Piezoelectric ceramics
Electrostrain
Structural transformation
Bifeo3-pbtio3
In-situ poling xrd

ABSTRACT

This study identifies the structural origin of giant electrostrain in samarium-doped bismuth ferrite lead titanate ($0.55Bi_{1-x}Sm_xFeO_3$–$0.45PbTiO_3$) ceramics. A giant peak-to-peak electrostrain (~0.5 % at 60 kV cm^{-1}) was obtained for compositions with x = 0.20 (20Sm) during initial poling, superior to $Pb(Zr,Ti)O_3$ based ceramics with similar phase transition temperature of 275 °C, coupled with a piezoelectric coefficient of 276 pC/N comparable with hard PZT. While 20Sm is a macroscopically pseudo-cubic relaxor in its unpoled state, an irreversible, field-induced transformation gives a tetragonal (c/a~1.115) ferroelectric phase as revealed by *in-situ* poling synchrotron X-ray diffraction and confirmed by transmission electron microscopy. The field-induced domain structure of the tetragonal structure could be reversibly switched under AC field after transformation. Quantitative strain analysis confirmed that the structural transformation accounts for approximately half of the total electrostrain, with the remainder by domain switching. These results highlight the importance of field-induced structural transformations for the development of high-performance piezoelectrics.

1. Introduction

Piezoelectric ceramics, characterised by their ability to interconvert electrical and mechanical energy, have been critical in the development of precision actuators, ultrasonic transducers and energy-harvesting systems in the 20th century. A central objective of electroceramic research is the achievement of large electrostrain to meet the requirements for high-displacement actuators in aerospace, robotics and biomedical applications. Lead zirconate titanate ($Pb(Zr,Ti)O_3$, PZT), which is currently the industry benchmark, gives an electrostrain of 0.1–0.2 % for compositions around the morphotropic phase boundary (MPB), [1,2] where the coexistence of rhombohedral and tetragonal phases facilitates efficient polarisation rotation and extension. However, some applications like actuators require greater electrostrain than typical PZT ceramics, which combined with environmental concerns regarding its substantial lead content (~60 wt %) have driven extensive efforts to identify alternative systems with superior electromechanical performance and lower Pb concentration [3]

Macroscopic large-signal electrostrain originates from both intrinsic and extrinsic contributions under the application of an external electric field [4] While all insulating materials exhibit a small degree of electrostrain due to the electrostrictive effect, ferroelectric (FE) and relaxor ferroelectric (REL) materials can yield significantly enhanced responses driven by domain switching and structural transformations, respectively. In typical FEs, macroscopic strain is dominated by the field-induced reorientation of domains and associated lattice strain. For example, in-situ electric field poling synchrotron X-ray diffraction and neutron diffraction studies on traditional PZT ceramics have successfully quantified the domain switching behaviour (e.g., via multiples of a random distribution) and contribution from intrinsic lattice strain [4,5] Alternatively, a phase transition or structural transformation induced by external electric fields often deliver a high electrostrain, particularly in lead-free systems such as $Na_{0.5}Bi_{0.5}TiO_3$ (NBT)-based ceramics [6–8] For example, an electrostrain of >0.3 % was obtained in NBT-0.02$NaNbO_3$

* Corresponding authors.
E-mail addresses: ge.wang@manchester.ac.uk (G. Wang), i.m.reaney@sheffield.ac.uk (I.M. Reaney).

https://doi.org/10.1016/j.actamat.2026.122480
Received 26 March 2026; Received in revised form 22 May 2026; Accepted 20 June 2026
Available online 24 June 2026

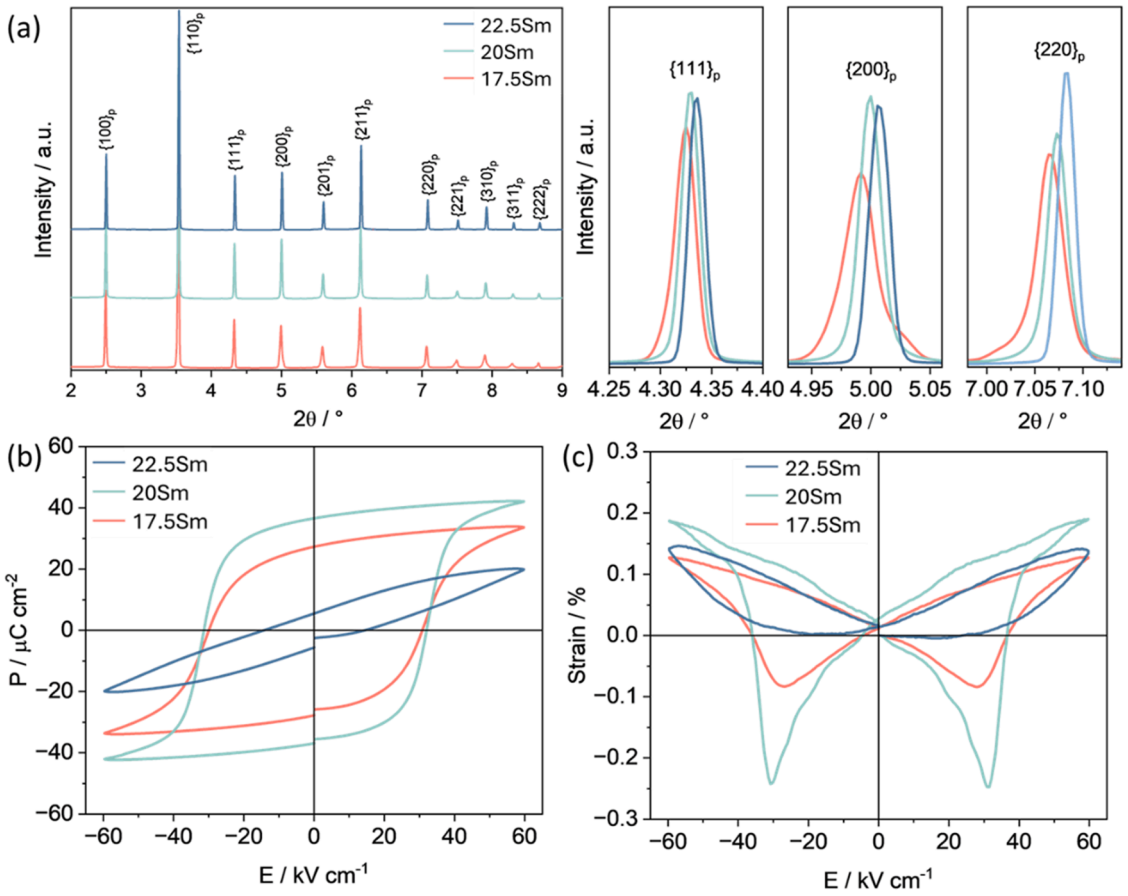

Fig. 1. (a) full-pattern SXRD of Sm doped BF-PT with close inspection on the $\{111\}_p$, $\{200\}_p$ and $\{220\}_p$ peaks. (b) Bipolar P-E and (c) S-E loops of Sm doped BF-PT ceramics.

(NBT-2NN) due to an irreversible structural transformation from a pseudocubic (*PC*) to a mixed structure of rhombohedral (*R*) and tetragonal (*T*) [9] An even higher strain (0.45 %) was reported in NBT-0.06$BaTiO_3$–0.02$K_{0.5}Na_{0.5}NbO_3$ (NBT-6BT-2KNN) attributed to a phase transition and subsequent strong domain switching [10] More recently electrostrains >1 % have been reported in various systems, including ones based on $BiFeO_3$ (BF), [11] NBT, [12] and KNN, [13] but these values necessitate rigorous structural validation. Longitudinal strain enhancements in piezoceramics can be significantly influenced by specimen geometry and bending deformations. For example, reducing the thickness of a PZT disc from 0.7 to 0.2 mm has been shown to result in a 300 % increase in the measured strain [14] Consequently, a comprehensive structural and microstructural characterisation is imperative to validate the origin of electromechanical responses, i.e. whether it arises from lattice, domain and structural effects or experimental artefacts.

Among all perovskite solid solutions, the $BiFeO_3$-$PbTiO_3$ (BF-PT) system is renowned for its large polarisation and high Curie temperature (T_C) at the MPB (T_C = 600–650 °C) [15] In 2018, Narayan et al. reported an electrostrain exceeding 1 % in 30 % La doped 0.55BF-0.45PT [11] The origin of such exceptionally high electrostrain was attributed to field-induced phase transition and subsequent domain dynamics, facilitated by the close match of the ionic radius of La^{3+} (1.36 Å) to that of Bi^{3+}. Building upon this framework, we explore the substitution of Sm^{3+}(1.24 Å) for Bi on the A site of BF-PT [16] We hypothesise that the smaller ionic radius of Sm^{3+} relative to La^{3+}(1.36 Å) will induce similar structural modifications and promote REL behaviour, thereby lowering the energy barrier for field-induced structural transitions and enhancing electrostrain [17] In this work, 0.55BF-0.45PT composition was selected to dope with Sm because it sits on the tetragonal side of the MPB, offering a high T_c and strong ferroelectric performance. The optimal composition compositions yield giant peak-to-peak bipolar strain ~0.5 % during initial poling and unipolar strain ~0.2 % during follow-on cycling, alongside a piezoelectric coefficient, d_{33} = 276 pC/N. *In-situ* electric field poling synchrotron X-ray diffraction is employed, coupled with transmission electron microscopy (TEM) to determine the structural origin of the giant electromechanical behaviour. The giant electrostrain benefits from an irreversible field-induced structural transformation and subsequent dynamic domain switching for compositions near the tetragonal to *PC* phase boundary (20Sm). The work not only explains and validates the origin of the giant electromechanical behaviour but also provides a mechanistic framework for the design of high-performance piezoelectric materials.

2. Experimental methods

$0.55Bi_{1-x}Sm_xFeO_3$–$0.45PbTiO_3$ (x = 0.175, 0.20 and 0.225, hereafter termed 17.5Sm, 20Sm and 22.5Sm) ceramics were synthesised via the conventional solid-state reaction method. High-purity oxide powders of Bi_2O_3 (>99.9 %, Sigma Aldrich), Fe_2O_3 (>99.95 %, Fisher Scientific), Sm_2O_3 (>99.9 %, Sigma Aldrich), PbO (>99.9 %, Sigma Aldrich), and TiO_2 (>99.9 %, Sigma Aldrich) were dried at 300 °C for 24 h prior to use. The precursors were weighed according to the stoichiometric formula and ball-milled in isopropyl alcohol with ZrO_2 milling media for 12 h. The resulting slurry was dried and calcined in air at 800 °C for 4 h, followed by a secondary milling step of 12 h to ensure chemical homogeneity. The calcined powders were mixed with a polyvinyl alcohol binder solution and uniaxially pressed into pellets. The green bodies were heated at 550 °C for 3 h to facilitate binder burnout and sintered in air at temperatures ranging from 1100 to 1200 °C for 2 h. The optimal

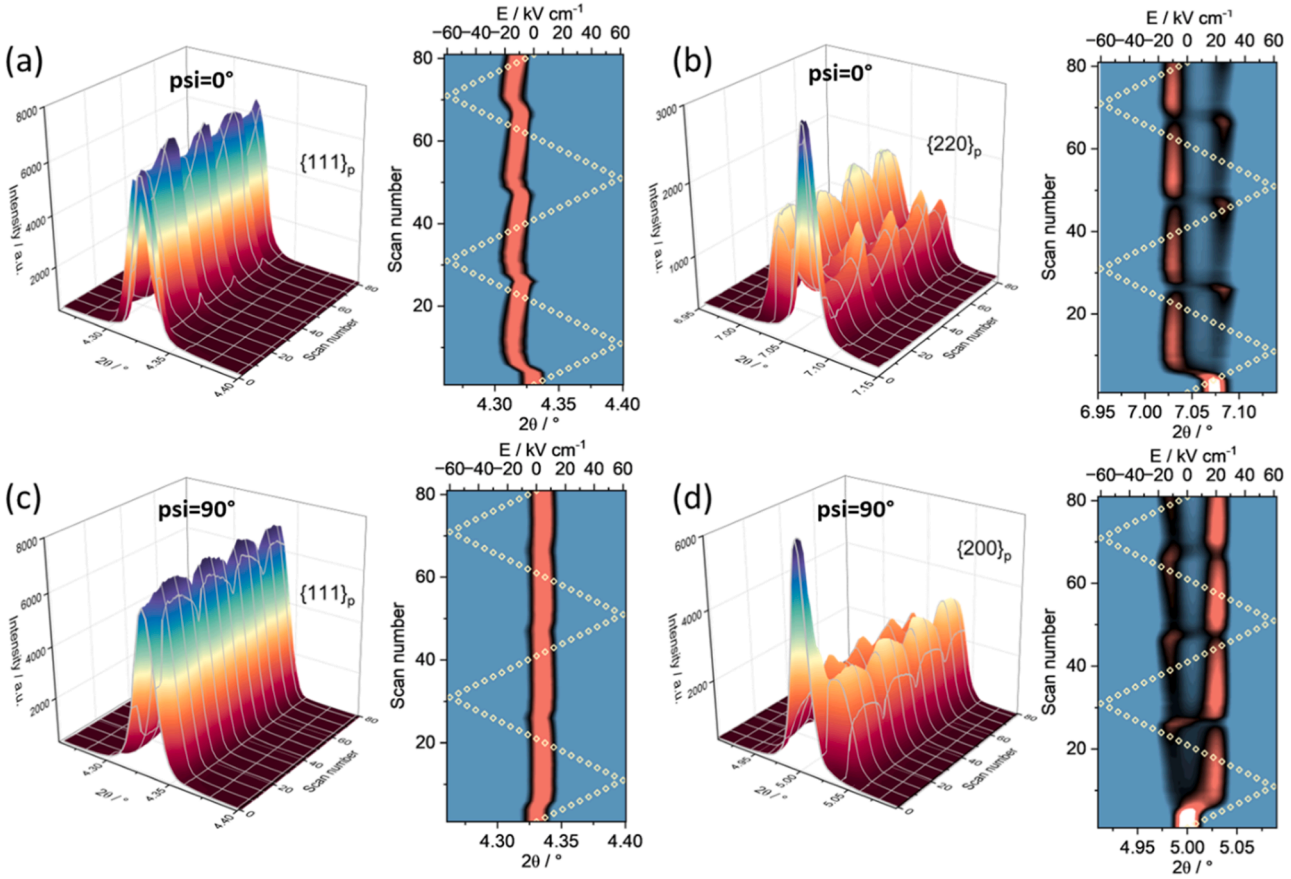

Fig. 2. 3D SXRD peak profile mapping and contour mapping of (a) $\{111\}_p$ at psi=0°, (b) $\{220\}_p$ at psi=0°, (c) $\{111\}_p$ at psi=90° and (d) $\{200\}_p$ at psi=90° during in-situ poling experiment.

sintering temperature for each composition was determined by evaluating the density of the sintered pellets using Archimedes method. The microstructure of the polished and thermally etched ceramics was analysed using a Nova Nano SEM 450 scanning electron microscope (FEI, USA).

For electrical characterisation, as-sintered ceramics were ground to a uniform thickness and coated with silver paste electrodes (Sunchemical, UK). Polarisation-electric field (P-E) and strain-electric field (S-E) hysteresis loops were recorded at 1 Hz using a ferroelectric tester (aixACCT TF 2000E). Temperature-dependent dielectric properties were obtained using an HP 4284A LCR meter (Agilent Technologies, USA) at frequencies of 1, 10 and 100 kHz. Piezoelectric d_{33} coefficient was measured using a Berlincourt meter. To evaluate quantitatively the electric field-induced structural transformations and domain switching behaviour, high-energy *in-situ* poling synchrotron X-ray diffraction was conducted at the Diamond Light Source (Beamline I15, UK) using a photon energy of 72 keV ($\lambda = 0.1722$ Å). Unpoled ceramic samples were machined into rectangular bars and mounted in a custom-designed polyimide holder immersed in silicone oil to prevent dielectric breakdown. The sample holder was electrically connected to a high-voltage amplifier (Matsusada EC-10, Japan). The X-ray beam was focused to ~120 μm × 76 μm. Two-dimensional (2D) diffraction patterns were collected in transmission geometry under applied electric fields up to 60 kV cm^{-1} using a Pilatus3 X CdTe 2 M detector positioned approximately 880 mm downstream of the sample. The beam was calibarated using LaB_6 and the exposure time for each image was 20 second. Two triangular AC cycles (both positive and negative fields) were completed on each specimen. The 2D images were segmented into conventional one-dimensional (1D) XRD patterns using DAWN [18] with a 15° step size in the azimuthal angle (psi) relative to the external electric field. Synchrotron X-ray diffraction peak positions and intensities were analysed using TOPAS 6 [19] Patterns corresponding to psi = 0° and psi = 90° represent diffractograms parallel and perpendicular to the direction of the applied electric field, respectively. Samples for transmission electron microscopy (TEM) were prepared by grinding the sintered ceramics and mixing them at a 1:10 ratio with fine aluminium powder (<10 μm) in acetone. The suspension was dried, placed between two aluminium foils, and cold-rolled to produce a thin composite sheet. This sheet was mechanically thinned, mounted onto a copper TEM grid using epoxy resin, and finally thinned to electron transparency via Ar^+ ion milling (Gatan PIPS II). Microstructural observation and selected area electron diffraction (SAED) were performed using a JEOL 2100 LaB_6 transmission electron microscope operated at 200 kV.

3. Results and discussion

The densities of all sintered pellets were measured using the Archimedes method to identify the optimum sintering temperature, which resulted in a relative density of > 93 % and dense microstructure (Figure S1, Supplemental Information). The crystal structure of the unpoled Sm-doped BF-PT ceramics were evaluated using synchrotron X-ray diffraction. As illustrated in Fig. 1a, all compositions exhibit a single perovskite structure without detectable secondary phases. A close inspection of the three synchrotron X-ray diffraction representative peaks, $\{111\}_p$, $\{200\}_p$ and $\{220\}_p$, reveals a composition-dependent structural evolution. For the 17.5Sm, the $\{200\}_p$ and $\{220\}_p$ peaks present a right and a left shoulder, respectively, indicative of a long-range ordered *T* symmetry. In contrast, increasing Sm content to 20 and 22.5 % results in the merging of these reflections into single, symmetric peaks, characteristic of a macroscopically *PC* structure. These data, alongside full-

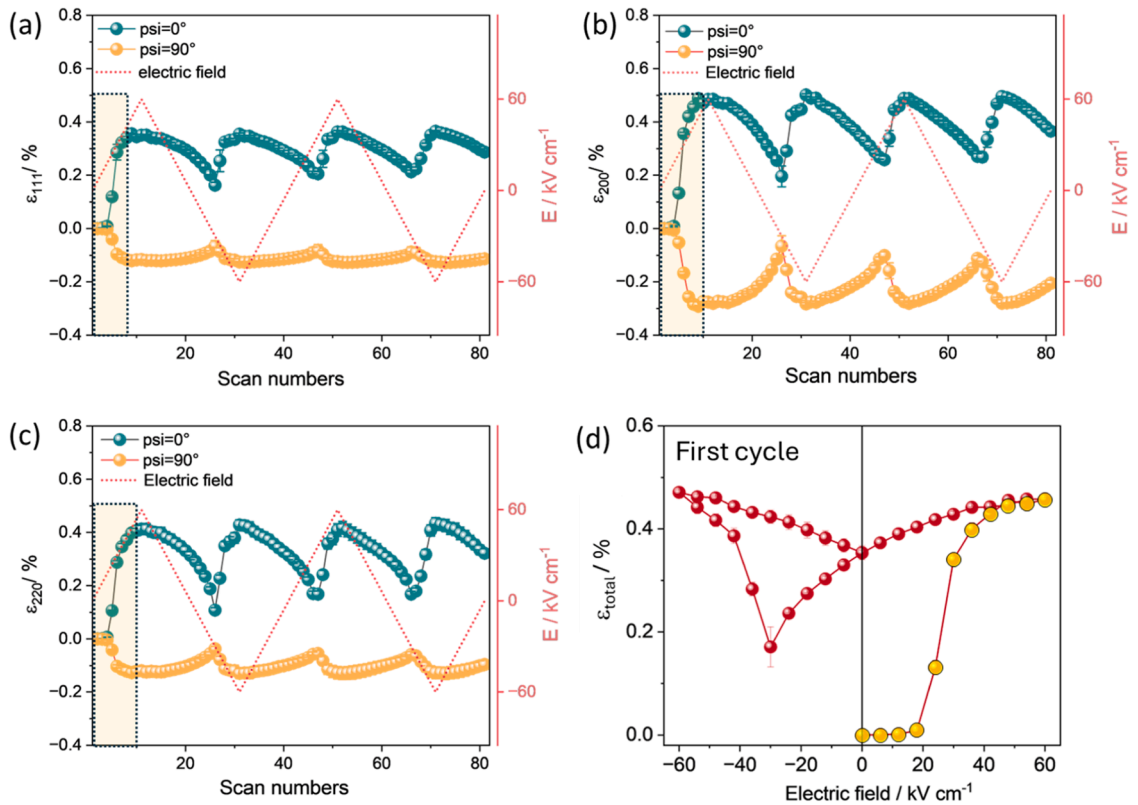

Fig. 3. $\{111\}_p$; (b)$\{200\}_p$; (c) $\{220\}_p$ and (d) total estimated strain (psi=0°) calculated from SXRD peaks during first cycle of applied field.

pattern Rietveld refinement results (Figure S2 and Table S1, Supplemental data), confirms a phase boundary at x = 0.2 (20Sm), separating the long-range FE from a *PC* REL state at room temperature. The macroscopic P-E and S-E hysteresis loops further corroborate this structural transition, Figs. 1b and 1c. The 17.5Sm ceramic exhibits a saturated P-E loop with a remnant polarisation (P_r)~ 30 μC cm^{-2} and a typical butterfly S-E loop with $+S_{max}$=0.13 % and $-S_{max}$=0.08 %. Notably, the 20Sm ceramic yields the highest maximum polarisation (P_{max})~40 μC cm^{-2} and P_r~36 μC cm^{-2}, alongside a giant peak-to-peak electrostrain of 0.46 %. Conversely, the 22.5Sm ceramic displays a significantly slimmer P-E loop with P_r<10 μC cm^{-2}, and an electrostrictive-like S-E loop with S_{max}=0.15 %, characteristic of REL behaviour. The combination of enhanced polarisation and giant electrostrain in the *PC*-structured 20Sm strongly suggests a field-induced REL to FE phase transition. We note that the phase boundary composition, 20Sm, exhibits a T_c at ~275 °C along with the onset of a frequency-dependent REL response, Figure S2d. To understand unambiguously the origins of the giant electrostrain and to rule out artefacts such as sample bending, *in-situ* electric field poling synchrotron X-ray diffraction was performed on 20Sm. By segmenting the 2D diffraction rings, the structural evolution parallel (psi = 0°) and perpendicular (psi = 90°) to the applied electric field was investigated, allowing for the direct observation of grain orientation effects, domain switching, and structural transformation.

Fig. 2 and Figure S3 (Supplemental information) display the 3D evolution of the $\{111\}_p$, $\{200\}_p$, and $\{220\}_p$ synchrotron X-ray diffraction profiles during two full cycles of electric field up to ±60 kV cm^{-1} with a step size of 6 kV cm^{-1}. In the initial state (scan 1), all three representative peaks at both psi = 0° and 90° appear as symmetric singlets at identical 2θ positions, confirming a macroscopically *PC* structure with random grain orientation. At psi = 0°, peaks shift towards lower 2θ (tensile strain), while at psi = 90°, they shift towards higher 2θ (compressive strain) under field. A critical structural transformation is observed as the field exceeds approximately 30 kV cm^{-1} during the first cycle. At psi = 0°, the $\{111\}_p$ peak remains a singlet but undergoes a pronounced shift, indicating a strong lattice deformation. We note that in a tetragonal phase the $\{111\}_p$ peaks do not split. Simultaneously however, the $\{200\}_p$ and $\{220\}_p$ peaks undergo clear splitting. Specifically, the $\{200\}_p$ peak develops a subtle right shoulder, Figure S3a (Supplemental data), whereas the $\{220\}_p$ peak exhibits a more obvious bifurcation into two distinct peaks, Fig. 2b At psi = 90°, the $\{200\}_p$ peak split into double, (200) and (002), Fig. 2d, immediately after the critical field with splitting of the $\{220\}_p$ peak less pronounced (Figure S3b, Supplemental data). The $\{111\}_p$ peaks as anticipated for a *T* phase remains singlet. During second cycle of AC poling, the peak intensities of the double $\{200\}_p$ and $\{220\}_p$ peaks vary dynamically with the field, Fig. 2b and 2d, corresponding to reversible domain switching from the field-induced FE structure. The changes on the SXRD peak profile, e.g., peak position, shape and intensities, provide direct crystallographic proof of a macroscopic transformation from a *PC*-structured REL phase to a long-range distorted (*T*) FE phase. At the end of two full AC cycles, the peak profiles do not return to their original singlet state upon field removal, confirming that the structural transformation is irreversible.

The estimated strains can be calculated from $\{111\}_p$, $\{200\}_p$, and $\{220\}_p$ synchrotron X-ray diffraction peaks using the methods described previously by Hall' group [20] and Daymond [21], and such strain analysis is the key to unlocking its origin and validating the macroscopic S-E measurement. The estimated tensile strains (first cycle) at psi=0°, ε_{111}, ε_{200}, ε_{220}, were found to be approximately 0.39, 0.51 and 0.42 %, respectively, Figure 3(a-c). Perpendicular to the external electric field at psi=90°, the estimated compressive strains of ε_{111}, ε_{200}, ε_{220} were obtained to be ε_{111}=−0.17 %, ε_{200}=−0.31 %, ε_{220}=−0.17 %, respectively, Figure 3(a-c). The most significant finding is the sharp increase (highlighted yellow regions) in all estimated strains during the initial poling cycle, which directly correlates with the field-induced irreversible structural transformation. The overall estimated macroscopic strain at psi=0° was calculated to be 0.48 % at 60 kV cm^{-1}, Fig. 3d, in agreement with the macroscopic S-E data (Fig. 1c). This quantitative convergence

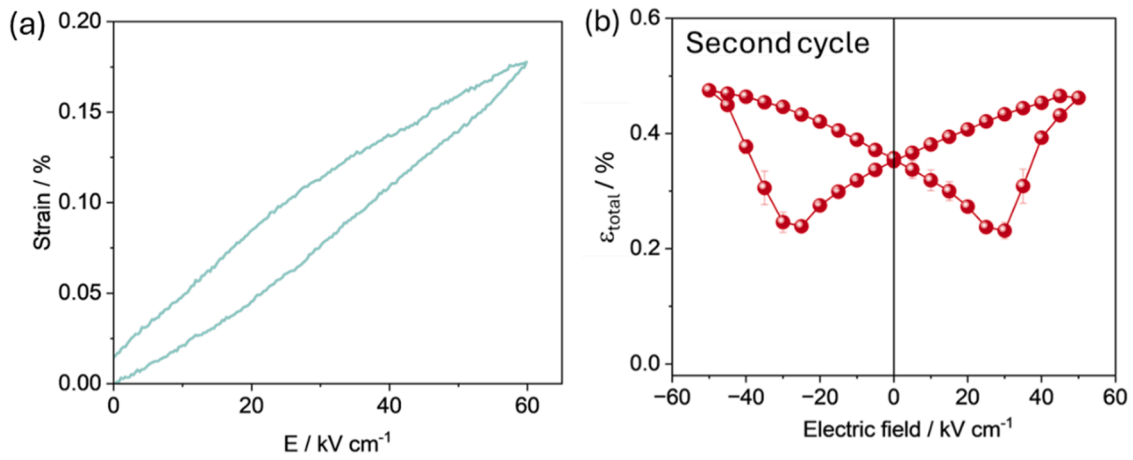

Fig. 4. (a) Unipolar S-E loop of 20Sm ceramics at steady state. (b) Total estimated strain (psi=0°) calculated from SXRD peaks during second cycle of applied field.

definitively proves that the giant electrostrain in 20Sm ceramics arise from structure, domain and lattice phenomena. The initial irreversible structural transformation from REL to FE contributes approximately 60 % of the total strain, while the other 40 % arises from domain switching from the field-induced FE phase. The initial electrostrain (~0.5 %) of 20Sm compositions is superior to PZTs of similar T_C and exhibits comparable d_{33} (230–350 pC/N) to hard PZT [22] ~30 % La is required to sufficiently destabilise the long-range *T* structure in previous research and induce a macroscopically *PC* structure [11,23] In this system, the long-range tetragonal order is destabilised at a lower concentration (~20 % Sm) than in La-doped counterparts. This is attributed to the smaller ionic radius of Sm^{3+} compared to La^{3+}. Specifically, using Shannon radii for 12-fold coordination, the substitution of Sm^{3+}(1.24 Å) for Bi^{3+} (~1.36 Å) creates an ionic size mismatch more than that of La^{3+} (1.36 Å). This greater size variance intensifies local lattice distortions and localised random fields, which more effectively disrupt the polar coupling. Consequently, the transition to a macroscopic *PC* state is facilitated at a lower dopant threshold. Theoretically, further decreasing the dopant radius should continue to reduce the critical concentration for destabilisation by enhancing random field strength. However, as the radius decreases there is an increasing risk that the ion will either not enter solid soultion, forming a second phase or it will reside on the B-site.

To further evaluate the potential of the 20Sm composition for high-displacement actuator applications, the stability of the electromechanical response and the underlying structural mechanism were investigated beyond the initial poling state (first cycle). As shown in Fig. 4a, the macroscopic unipolar strain reaches a stable value of approximately 0.18 % at 60 kV cm^{-1} during the second cycle and after, directly linked to the stabilised ferroelectric tetragonal phase. While giant peak-to-peak strain (~0.5 %) was obtained during 'virgin' cycle due to a massive structural transformation from a pseudo-cubic to a tetragonal phase (Fig. 3d), the *in-situ* synchrotron XRD data during second cycle, Fig. 4b, demonstrates that the material remains in this newly formed tetragonal state with intrinsic piezoelectric response and domain switching. Unlike ergodic relaxor systems, such as NBT-based ceramics, [9,10] which often suffer from functional fatigue due to the constant stress of reversible phase switching, the Sm-doped BF-PT system operates via the intrinsic piezoelectricity of a stabilised phase during subsequent cycling. This transition from an initial giant structural jump (~0.5 % bipolar peak-to-peak) to a consistent, steady-state actuation strain (~0.2 % unipolar) provides a foundation for structural reliability in long-term applications. The 20Sm composition serves as a viable 'lead-light' alternative to conventional PZT by significantly reducing the lead mass fraction through $BiFeO_3$ substitution (55 at% $Bi/SmFeO_3$). While standard hard PZTs with similar thermal stability (T_C~250 °C) typically

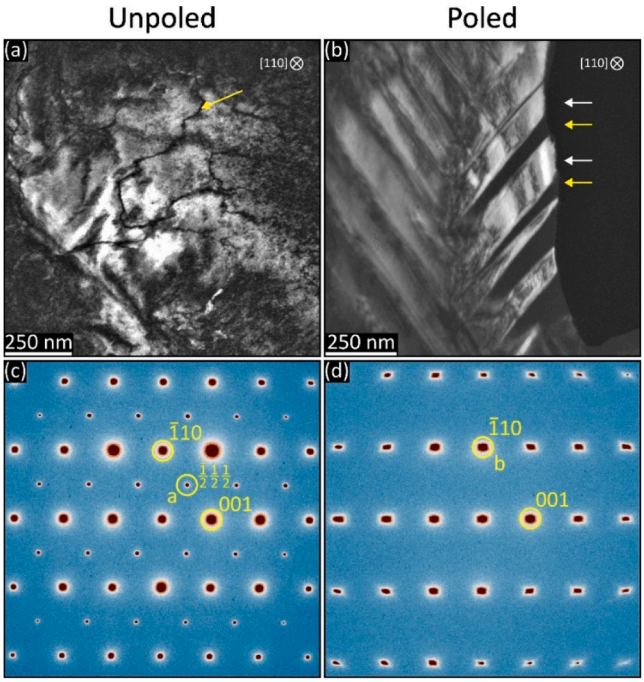

Fig. 5. Dark field TEM and electron diffraction of the samples. Dark field micrographs of the unpoled (a) and poled (b) samples, formed from the circled diffraction spots in (c) and (d), respectively. Arrows point to antiphase boundary in (a) and twin domains in (b). Electron diffraction patterns for the unpoled (c) and poled (d) samples, illustrating the presence of superstructure spots in the unpoled material. All notation respective to the prototype cubic perovskite cell.

yield unipolar strains ~0.1 %, the 20Sm composition achieves a superior initial bipolar strain of ~0.5 % and better steady-state unipolar strain of ~0.2 % with a T_C of 275 °C. Furthermore, our *in-situ* poling synchrotron XRD data confirms that this performance is achieved via a stabilised tetragonal phase, ensuring that the enhanced strain is maintained without the structural degradation often associated with repeated phase transition.

Electron microscopy was used to further verify the domain structure of the poled and virgin (unpoled) ceramic materials. Fig. 5 illustrates microstructural differences between the two materials, where Fig. 5a and 5b are dark field micrographs of the unpoled and poled 20Sm ceramics, respectively. The corresponding [110] direction diffraction patterns are presented in Fig. 5c and Fig. 5d, in which the spots used to form

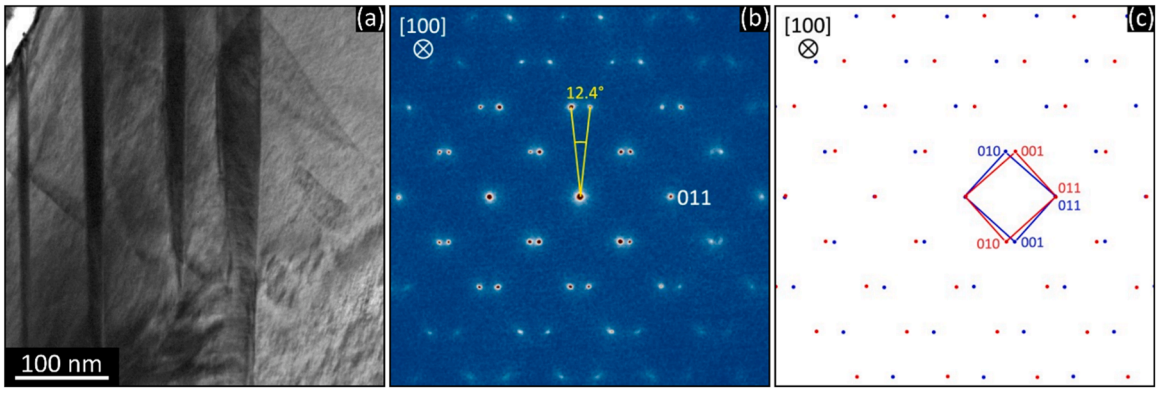

Fig. 6. Electron microscopy of the poled sample. (a) Bright field micrograph showing the presence of twin domains. (b) Electron diffraction pattern and (c) schematic of a region encompassing two twin domains, illustrating the tetragonal distortion.

the dark field micrographs are circled and indicated by letters. The diffraction pattern of the virgin (unpoled) sample contains $\left(\frac{1}{2}\frac{1}{2}\frac{1}{2}\right)$ superstructure spots, indicative of a larger supercell than the standard cubic perovskite cell. The emergence of $\left(\frac{1}{2}\frac{1}{2}\frac{1}{2}\right)$ superstructure spots are related to out-of-phase tilting of the BO_6 octahedra along at least one of the principal axes of the cubic prototype cell and most likely are associated with a rhombohedral (R), $a^-a^-a^-$ tilt system based on the crystal chemistry of the $BiFeO_3$ (R3c, $a^-a^-a^-$) end member [24] We speculate that the long-range tilting in the unpoled state is not strongly coupled with cation displacements, hence XRD data exhibits a *PC* rather than *R* structure in average Rietveld refinements.

The contrast in the dark field micrograph presented in Fig. 5a shows the presence of antiphase boundaries which appear as dark lines (see arrow) and arise from tilted regions which have nucleated and impinged out of phase. The diffraction pattern of the poled material in Fig. 5d does not exhibit any superstructure spots, consistent with a tetragonal P4mm cell. The microstructure of the poled material shows a clear twin domain structure with orientational preference, forming alternating bright and dark regions illustrated by arrows in Fig. 5b To further investigate the twin domains, the poled material was also imaged in the [100] direction. Fig. 6a shows a bright-field micrograph where the domains are visible. The associated diffraction pattern presented in Fig. 6b is recorded from a region encompassing both the bright and dark domains. As can be seen in Fig. 6b and the schematic in Fig. 6c, there are therefore two separate patterns present. The domains share a common (011) plane, which can be used to measure the distortion of the lattice. Based on the angular difference between the spots in the two domains, the cell was established to be tetragonal with a c/a ratio of 1.115. This persistent high tetragonality provides a larger potential for domain switching and lattice strain, directly contributing to the superior piezoelectric sensitivity observed in the poled 20Sm composition.

4. Conclusion

In summary, Sm doped BF-PT ceramics were successfully synthesised, with the 20Sm exhibiting a giant peak-to-peak bipolar strain of ~0.5 % (initial), a unipolar strain ~0.2 % (steady state) coupled with d_{33} = 276 pC/N, a potential candidate for actuator applications. By employing *in-situ* electric field poling SXRD and TEM, we demonstrate that the giant electrostrain originates from an irreversible phase transition from a REL to a FE state, as evident by a structural transformation from a *PC* to a *T* symmetry with an exceptionally large c/a ratio of 1.115. Our quantitative analysis unlocks the origin of this strain, partitioning it equally between the initial irreversible structural transformation and subsequent reversible domain switching. This work not only presents a ceramic with giant electrostrain but also describes a rigorous mechanistic framework for the design and validation of next-generation, high-performance piezoelectrics.

CRediT authorship contribution statement

Xinzhen Wang: Methodology, Investigation, Formal analysis, Data curation, Conceptualization. **Hareem Zubairi:** Methodology, Investigation, Formal analysis, Data curation. **Robin Sjökvist:** Software, Methodology, Investigation, Data curation. **Muhammad Wasim:** Methodology, Investigation, Formal analysis, Data curation. **Xiaojiao Liu:** Methodology, Investigation, Formal analysis, Data curation. **Annette K. Kleppe:** Software, Project administration, Methodology, Investigation, Data curation. **Antonio Feteira:** Resources, Methodology, Investigation. **Richard Beanland:** Software, Resources, Methodology, Investigation, Formal analysis, Data curation. **Ge Wang:** Writing – review & editing, Writing – original draft, Visualization, Validation, Supervision, Software, Resources, Project administration, Methodology, Investigation, Funding acquisition, Formal analysis, Data curation, Conceptualization. **Ian M Reaney:** Writing – review & editing, Writing – original draft, Supervision, Resources, Project administration.

Declaration of competing interest

The authors declare that they have no known competing financial interests or personal relationships that could have appeared to influence the work reported in this paper.

Acknowledgements

This work was supported by the Engineering and Physical Sciences Research Council (EP/Z536003/1) and China Scholarship Council (No. 202008370166). Ge Wang and Hareem Zubairi would like to acknowledge the financial support from the Dame Kathleen Ollerenshaw Fellowship and Dean's scholarship provided by The University of Manchester. We also thank Diamond Light Source for access to beamline I15 (proposal numbers CY36011-1 and CY39563-1), the wider support provided by the Functional Materials and Devices group at The University of Sheffield and David A. Hall (The University of Manchester) for assistance with sample testing.

Supplementary materials

Supplementary material associated with this article can be found, in the online version, at doi:10.1016/j.actamat.2026.122480.

References

[1] T.R. Shrout, S.J. Zhang, Lead-free piezoelectric ceramics: alternatives for PZT? J. Electroceramics 19 (1) (2007) 113–126.

[2] Z. Gubinyi, C. Batur, A. Sayir, F. Dynys, Electrical properties of PZT piezoelectric ceramic at high temperatures, J. Electroceramics 20 (2) (2008) 95–105.

[3] J. Rodel, W. Jo, K.T.P. Seifert, E.-M. Anton, T. Granzow, D. Damjanovic, Perspective on the development of lead-free piezoceramics, J. Am. Ceram. Soc. 92 (6) (2009) 1153–1177.

[4] J.L. Jones, E.B. Slamovich, K.J. Bowman, Domain texture distributions in tetragonal lead zirconate titanate by x-ray and neutron diffraction, J. Appl. Phys. 97 (3) (2005) 034113.

[5] D.A. Hall, L. Daniel, A. Stoica, K. An, H. Skorpenske and P.J. Withers, *In-situ* neutron diffraction analysis of PZT ceramics under combined electrical and mechanical loading. *Electroceramics for End-users VII conference (PIEZO2015)*, 2015, Maribor, Slovenia. ⟨hal-01245635⟩.

[6] J. Rodel, J. Li, Lead-free piezoceramics: status and perspectives, MRS Bull. 43 (8) (2018) 576–580.

[7] H. Zubairi, G. Wang, Electric field-induced phase transition behaviour in sodium bismuth titanate-based ceramics, Adv. Energy Sustaina. Res. 7 (2026) e202500495.

[8] G. Viola, Y. Tian, C. Yu, Y. Tan, V. Koval, X. Wei, K.-L. Choy, H. Yan, Electric field-induced transformations in bismuth sodium titanate-based materials, Prog. Mater. Sci. 122 (2021) 100837.

[9] G. Wang, Z. Lu, Z. Zhang, A. Feteira, C.C. Tang, D.A. Hall, Electric field-induced irreversible relaxor to ferroelectric phase transformations in $Na_{0.5}Bi_{0.5}TiO_3$-$NaNbO_3$ ceramics, J. Am. Ceram. Soc. 102 (12) (2019) 7746–7754.

[10] S.-T. Zhang, A.B. Kounga, E. Aulbach, H. Ehrenberg, J. Rödel, Giant strain in lead-free piezoceramics $Bi_{0.5}Na_{0.5}TiO_3$-$BaTiO_3$-$K_{0.5}Na_{0.5}NbO_3$ system, Appl. Phys. Lett. 91 (11) (2007) 112906.

[11] B. Narayan, J.S. Malhotra, R. Pandey, K. Yaddanapudi, P. Nukala, B. Dkhil, A. Senyshyn, R. Ranjan, Electrostrain in excess of 1% in polycrystalline piezoelectrics, Nat. Mater. 17 (5) (2018) 427–431.

[12] H. Luo, H. Liu, H. Huang, Y. Song, M.G. Tucker, Z. Sun, Y. Yao, B. Gao, Y. Ren, M. Tang, H. Qi, S. Deng, S. Zhang, J. Chen, Achieving giant electrostrain of above 1% in (Bi,Na)TiO_3-based lead-free piezoelectrics via introducing oxygen-defect composition, Sci. Adv. 9 (5) (2023) eade7078.

[13] G. Huangfu, K. Zeng, B. Wang, J. Wang, Z. Fu, F. Xu, S. Zhang, H. Luo, D. Viehland, Y. Guo, Giant electric field-induced strain in lead-free piezoceramics, Science 378 (6624) (2022) 1125–1130.

[14] G.D. Adhikary, A. Adukkadan, G.J. Muleta, R.P.S. Monika, D.N. Singh, H. Luo, G. A. Tina, L. Giles, S. Checchia, J. Daniels, R. Ranjan, Longitudinal strain enhancement and bending deformations in piezoceramics, Nature 637 (8045) (2025) 333–338.

[15] H. Amorín, C. Correas, C.M. Fernández-Posada, O. Peña, A. Castro, M. Algueró, Multiferroism and enhancement of material properties across the morphotropic phase boundary of $BiFeO_3$-$PbTiO_3$, J. Appl, Phys. 115 (10) (2014) 104104.

[16] R.D. Shannon, Revised effective ionic radii and systematic studies of interatomic distances in halides and chalcogenides, Acta Cryst. 32 (1976) 751–767.

[17] X. He, T. Wang, X. Li, S. Das, X. Liu, Z. Chen, Enhanced piezoelectricity and excellent thermal stability in Sm^{3+}-doped $BiFeO_3$-$PbTiO_3$ ceramics, ACS Appl. Electron. Mater. 4 (2) (2022) 807–813.

[18] M. Basham, J. Filik, M.T. Wharmby, P.C.Y. Chang, B.E. Kassaby, M. Gerring, J. Aishima, K. Levik, B.C.A. Pulford, I. Sikharulidze, D. Sneddon, M. Webber, S. S. Dhesi, F. Maccherozzi, S. Brockhauser, G. Naray, A.W. Ashton, Data analysis WorkbeNch (DAWN), J. Synchrotron Rad. 22 (2015) 853–858.

[19] A.A. Coelho, TOPAS and TOPAS-Academic: an optimization program integrating computer algebra and crystallographic objects written in C++, J. Appl. Cryst 51 (2018) 210–218.

[20] Y. Li, Y. Chen, Z. Zhang, A. Kleppe, D.A. Hall, In-situ XRD study of actuation mechanisms in $BiFeO_3$-$K_{0.5}Bi_{0.5}TiO_3$-$PbTiO_3$ ceramics, Acta Mater. 168 (2019) 411–425.

[21] M.R. Daymond, The determination of a continuum mechanics equivalent elastic strain from the analysis of multiple diffraction peaks, J. Appl. Phys. 96 (2004) 4263–4272.

[22] Piezoelectric bulk piezoceramics: Ceramic material properties datasheet (2021). https://www.ctscorp.com/Files/DataSheets/Piezoelectric/Bulk-Piezoceramics/CTS-Piezoelectric-Bulk-Piezoceramics-Ceramic-Material-Properties-Datasheet.pdf.

[23] T. Leist, T. Granzow, W. Jo, J. Rödel, Effect of tetragonal distortion on ferroelectric domain switching: a case study on La-doped $BiFeO_3$-$PbTiO_3$ ceramics, J. Appl. Phys. 108 (1) (2010) 014103.

[24] A. Glazer, The classification of tilted octahedra in perovskites, Acta Crystallogr. Section B 28 (11) (1972) 3384–3392.